Supplementary Information (SI) for Journal of Materials Chemistry A.
This journal is © The Royal Society of Chemistry 2025

Supporting Information

Interfacial Tautomerization Modulated S-scheme MOF/COF Heterojunctions for Enhanced Photocatalytic H_2O_2 Production

Zhu Gao[a*], Yan Xu[a], Zeyu Sun[a], Zhenglin Li[a], Fuhua Li[a], Guipeng Yu[b*] and Cuijuan Wang[a*]

[a]School of chemistry, Southwest Jiaotong University 610031 Chengdu, Sichuan, P. R. China

[b]College of Chemistry and Chemical Engineering, Central South University 410083 Changsha, Hunan, P. R. China

`

*Corresponding author: Zhu Gao, E-mail: gaozhu@swjtu.edu.cn; Cuijuan Wang, E-mail: wangcuijuan@swjtu.edu.cn; Guipeng Yu, E-mail: gilbertyu@csu.edu.cn

Experimental Procedures

Synthesis of amino functional UiO-66

Preparation of UiO-66: 31.5 mg of $ZrCl_4$ and 26.4 mg of ATA were put into a stainless-steel reactor containing 10 mL of DMF and 1.2 mL of acetic acid. After thorough mixing, it was heated at 120 °C for 24 hours. A white product was obtained, which was collected by centrifugation and washed with DMF and ethanol three times respectively. The product was dried in a vacuum oven at 80 °C overnight (80% yield). The resulting samples were denoted as UiO-66.

Synthesis of Tp-COF

Preparation of Tp-COF: 58.4 mg of TTBA and 24 mg of Tp were placed in a 50 mL of Pyrex tube containing 1 mL of butanol, 1 mL of mesitylene and 0.2 mL (6 M) of acetic acid. Subsequently, the Pyrex tube was placed onto a sonic bath for 20 minutes to obtain a homogeneous mixture. Next, vacuum the Pyrex tube with a vacuum pump to remove oxygen. Finally heated at 120°C for 72 hours. A yellow product was obtained, which was collected by centrifugation, and washed three times each with THF and acetone, respectively. The obtained solid was then soaked in THF for 48 h. The obtained product was dried overnight in a vacuum oven at 80°C (92% yield).

Photocatalytic performance measurements

The 10 mg as-prepared heterojunction photocatalyst was thoroughly dispersed in 80 mL 2.5% triethylamine solution via ultrasonication for 10 minutes. The resulting mixture was then transferred to a reaction flask and irradiated under visible light ($\lambda >$ 420 nm) using a 300 W xenon lamp (Microsolar 300, Beijing Perfectlight) equipped with a cutoff filter. The reaction was conducted under air atmosphere with continuous stirring. Circulating cooling water was used to maintain the reaction temperature at 25 °C. After irradiation, 1 mL of the reaction solution was sampled with a syringe and filtered through a 0.2 μm Millipore membrane to remove the photocatalyst. The concentration of produced H_2O_2 was quantified using the KI titrimetric method.[1]

$$H_2O_2 + I^- \rightarrow I_3^- + H_2O$$

Hydrogen peroxide oxidizes I^- to yellow I_3^-, and the absorbance of I_3^- at 352 nm is detected by UV-vis spectro-photometer, and the concentration of produced H_2O_2 can be obtained according to the standard curve. Thus, the concentration of produced H_2O_2 could be calculated by the following equation:

$$c(H_2O_2) = c(I_3^-)$$

A series of I_3^- solutions with varying concentrations were prepared, and the absorbance values at 352 nm were measured by UV-vis spectrophotometer. The relationship between absorbance and concentration was obtained by linear simulation, as illustrated below:

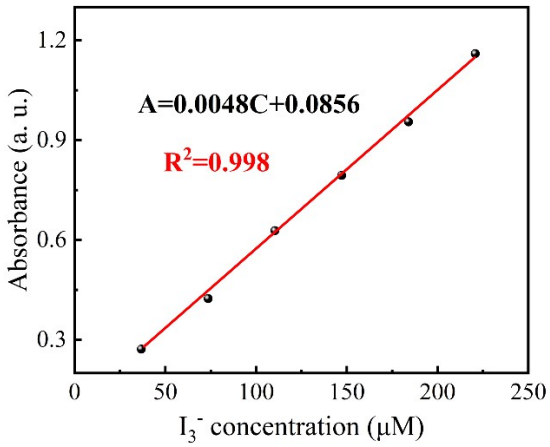

Scheme S1. Calibration curve

According to the calibration curve of I_3^- concentration and the absorption intensity, the concentration of produced H_2O_2 could be calculated.

DFT calculations

Density functional theory (DFT) calculations were carried out using the exchange-correlation function and CASTEP module. The HSE06 hybrid functional was used to obtain the band structure. An energy cutoff of 750 eV and a Monkhorst-Pack k-point mesh of 4 × 4 × 1 were used to perform geometry optimization and electronic property calculations. The energy and force convergence criteria were set as 1.0×10^{-5} eV per atom and 0.03 eV $Å^{-1}$, respectively. A vacuum space of 20 Å was used. The work function (Φ) is calculated using $\Phi = E_{Vac} - E_F$, where E_{Vac} is the electrostatic potential of the vacuum level and E_F is the Fermi energy.

We carried out the DFT calculations in the standard Gaussian 16 software package[[2]]. Following which, the calculations of geometry optimization was carried out by using the PBE-D3(BJ)[[3, 4]] (including London-dispersion correction) function with the 6-311G(d) basis set for all atoms. The vibrational frequency is subsequently carried out at the same level as geometry optimization for characterising the nature of the stationary point that all frequencies of local minimum is positive and for free energy calculation. In addition, the single-point energy of studied stationary point is calculated by using the PBE-D3(BJ) function with the 6-311G(d,p) basis set for all atoms.

The associative mechanism for two-electron ORR comprises sequential addition of a proton and electron in each step, shown as below:

$$* + O_2 + H^+ + e^- \rightarrow *OOH \qquad (1)$$

$$*OOH + H^+ + e^- \rightarrow * + H_2O_2 \qquad (2)$$

The asterisk (*) denotes the active site on catalyst.

In addition, the molecular orbital localization analysis related.

Results and Discussion

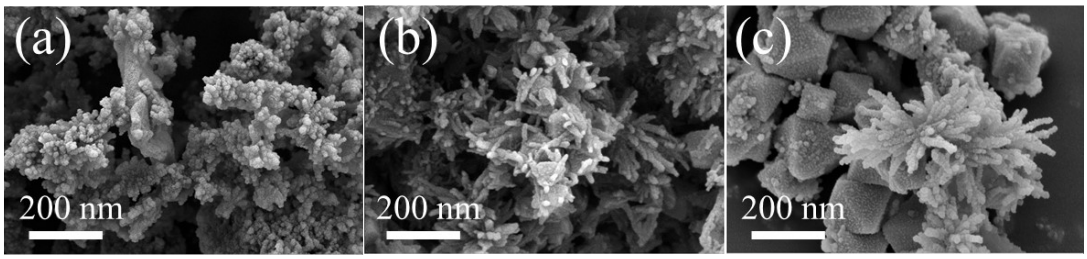

Fig. S1 SEM image of (a) UiO-66@Tp-$COF_{0.5}$, (b) UiO-66@Tp-COF_1 and (c)UiO-66@Tp-$COF_{1.5}$.

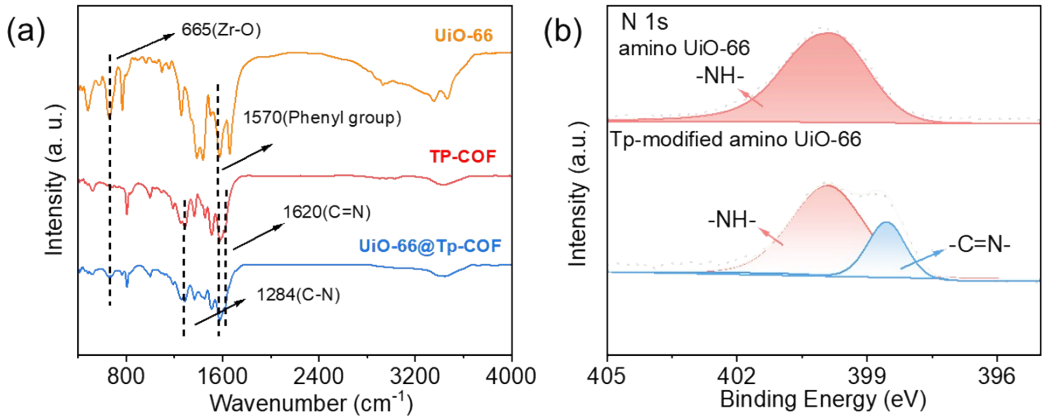

Fig. S2. (a) Fourier transform infrared (FT-IR) spectra of UiO-66, Tp-COF, and UiO-66@Tp-COF$_1$. (b) N 1s spectra for amino UiO-66 and Tp-modified amnio UiO-66.

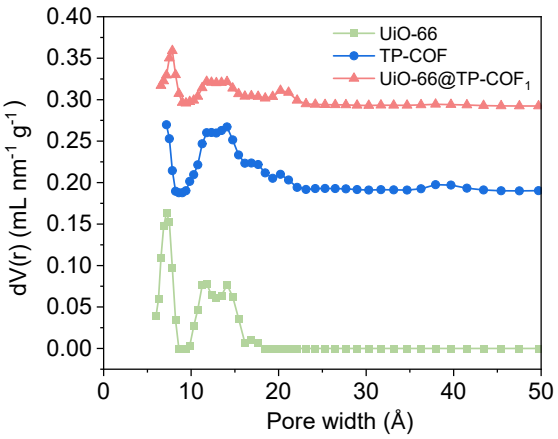

Fig. S3. The pore size distribution analyses of UiO-66, Tp-COF, and UiO-66@Tp-COF_1.

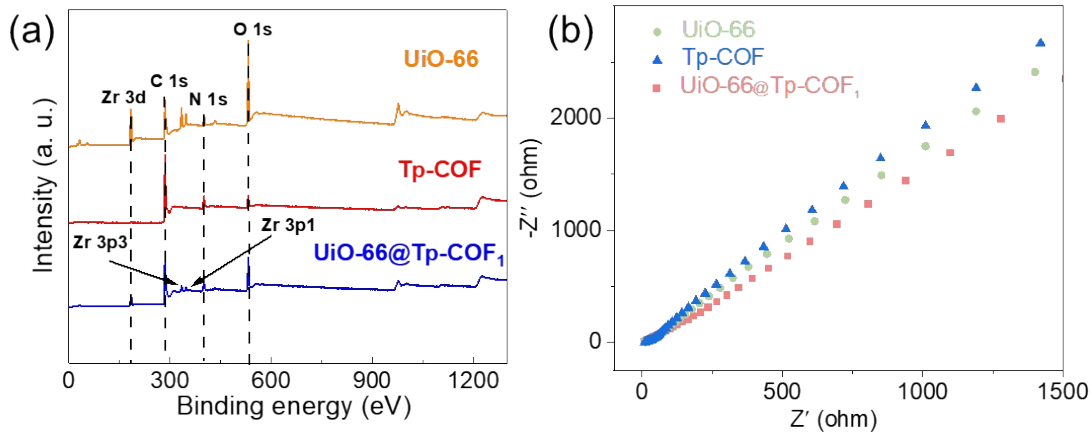

Fig. S4. (a) X-ray photoelectron spectroscopy (XPS) and (b) electrochemical impedance spectroscopy (EIS) of Tp-COF, UiO-66 and UiO-66@Tp-COF$_1$.

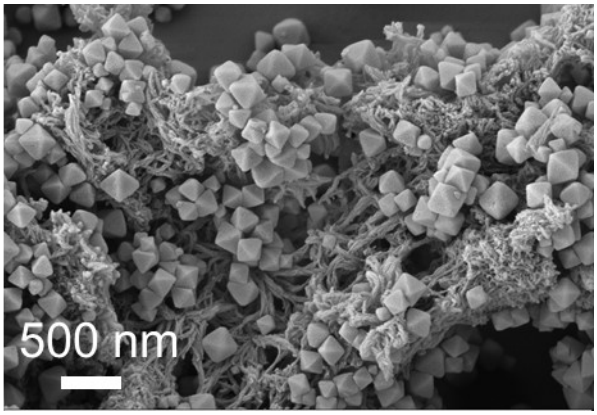

Fig. S5. SEM images of UiO-66+Tp-COF_1.

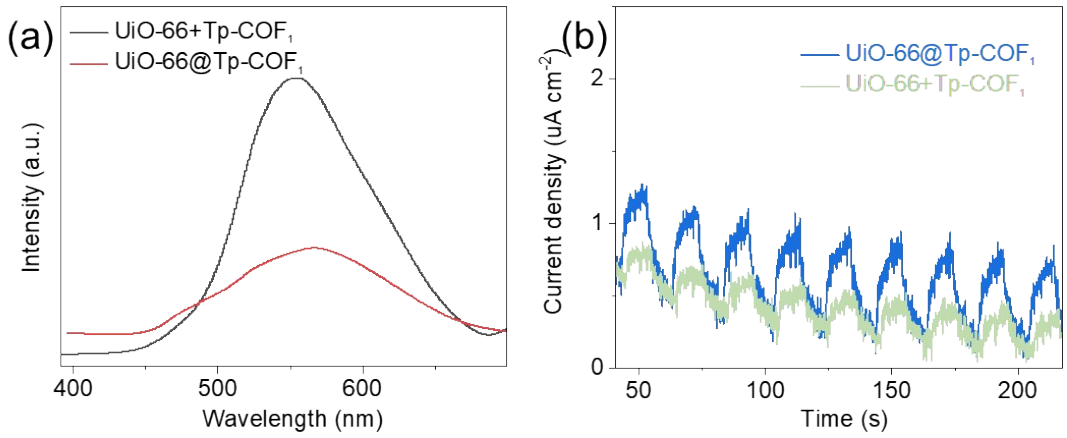

Fig. S6. (a) photoluminescence spectra (PL, excited at 375 nm) and (b) Photocurrent response of UiO-66+Tp-COF_1 and UiO-66@Tp-COF_1.

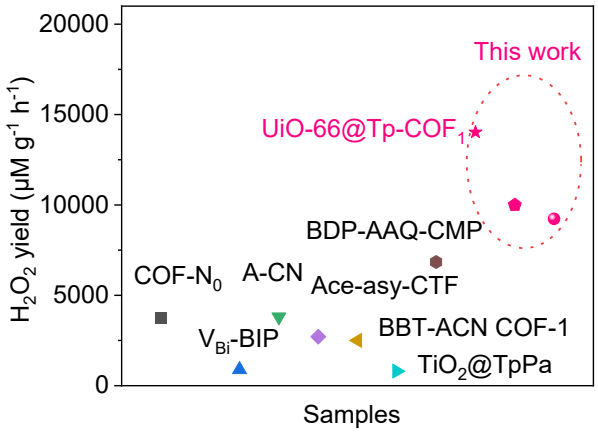

Fig. S7. Photocatalytic H_2O_2 production performance on the reported photocatalysts.[5-14]

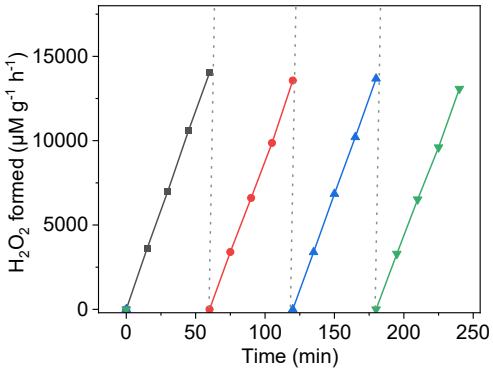

Fig. S8. Performance of UiO-66@Tp-COF_1 for four consecutive cycles of H_2O_2 production.

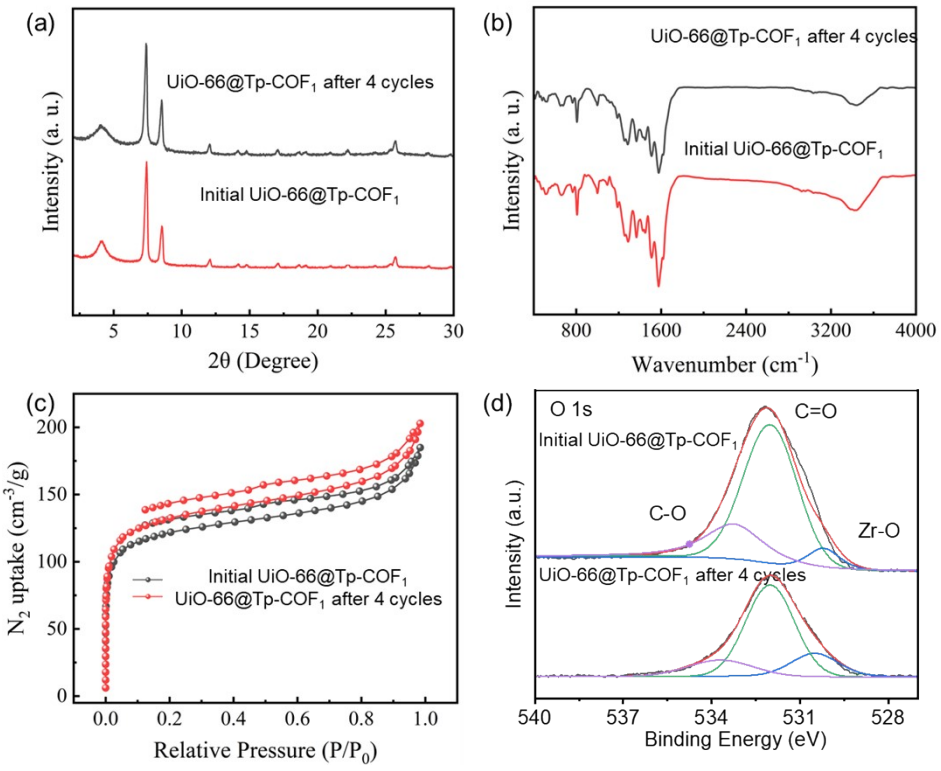

Fig. S9. (a) XRD patterns, (b) FT-IR spectra, (c) N_2 sorption isotherms, and (d) XPS O 1s spectra of the UiO-66@Tp-COF_1 before and after reaction cycles.

We compared the high-resolution O 1s spectra of the fresh and used UiO-66@Tp-COF_1 catalyst after four consecutive reaction cycles. The spectra show negligible shifts in the binding energies and no significant changes in the relative ratios of the characteristic peaks (e.g., C-O, C=O, Zr-O). This indicates that the chemical states of the key elements, particularly the interfacial imine bonds and the keto-enamine tautomers, remain intact. We compared the FTIR spectra of the catalyst before and after the reaction. The characteristic absorption bands remain virtually unchanged. Specifically, the bands corresponding to the C=N stretch (around 1620 cm^{-1}) and the C=C bonds (from the aromatic rings and tautomers) show no signs of degradation or shift. The post-reaction XPS and FTIR analyses provide strong evidence that the UiO-66@Tp-COF_1 heterojunction is a highly stable catalyst. The active sites (the keto-enamine tautomers at the interface) are not consumed or permanently altered during the reaction. This suggests that the mechanism involves a catalytic cycle where the active sites facilitate the reduction of O_2 to H_2O_2 and are regenerated.

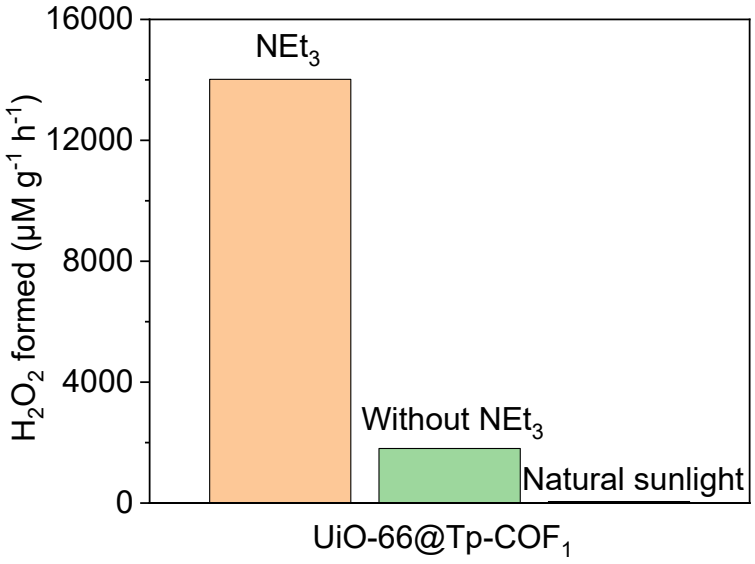

Fig. S10. The controlled experiments of H_2O_2 generation under different scavengers for UiO-66@Tp-COF_1.

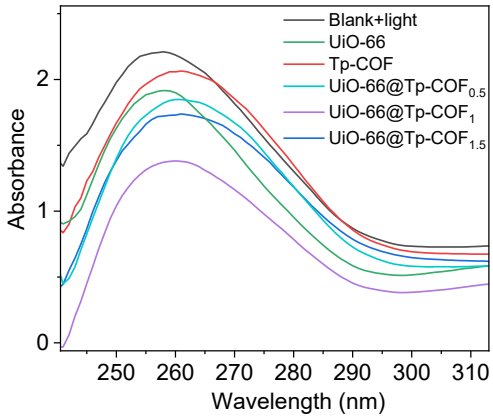

Fig. S11. UV−vis absorption spectra of the nitroblue tetrazolium generated by samples in the presence of light and oxygen.

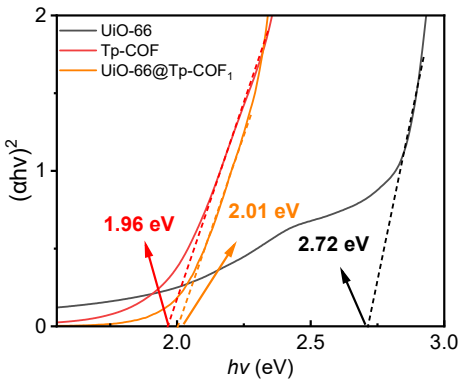

Fig. S12. Kubelka-Munk function vs. the energy of incident light plots in Tp-COF, UiO-66 and UiO-66@Tp-COF_1.

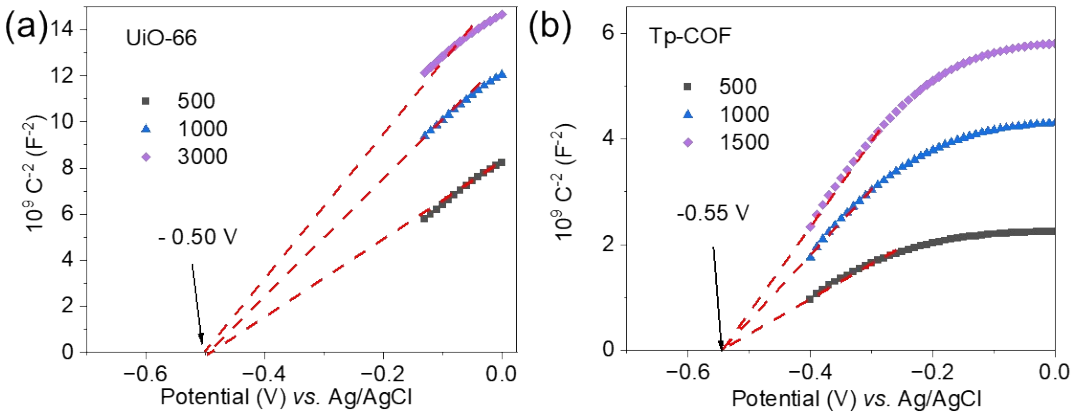

Fig. S13. Mott-Schottky plots of (a) UiO-66 and (b) Tp-COF.

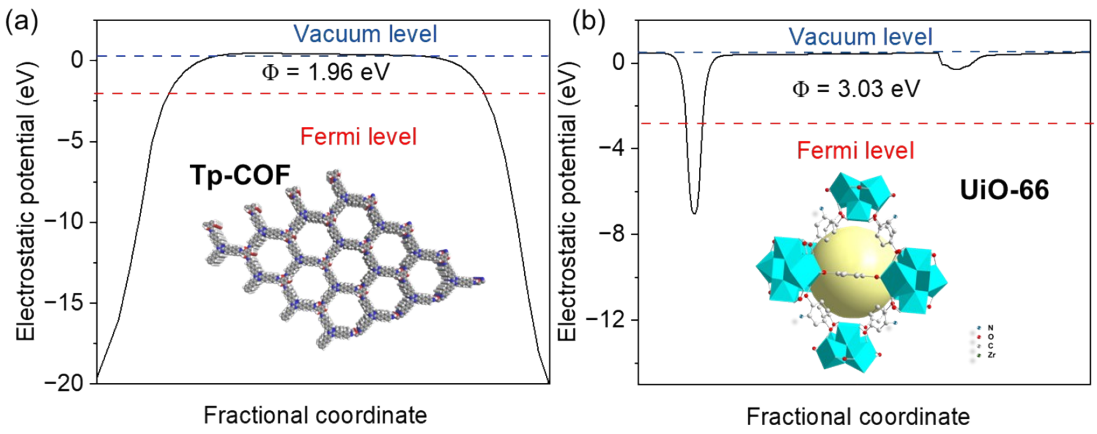

Fig. S14. The calculated work function and corresponding structures of (a) UiO-66 and (b) Tp-COF

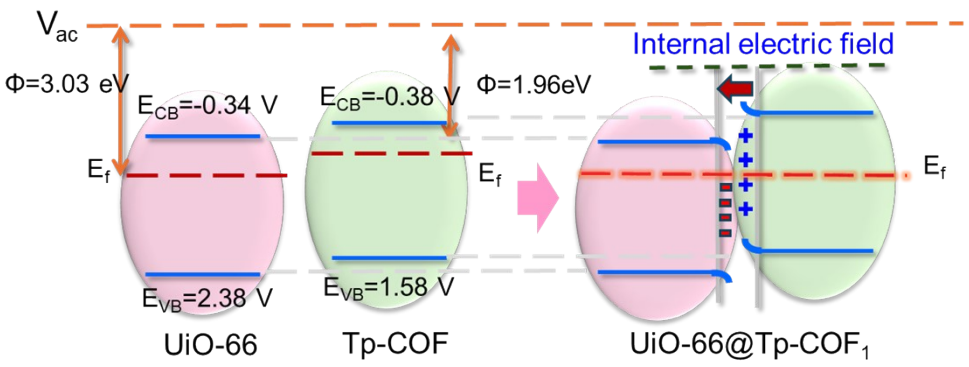

Fig. S15. Band structure of Tp-COF, UiO-66 and heterojunction.

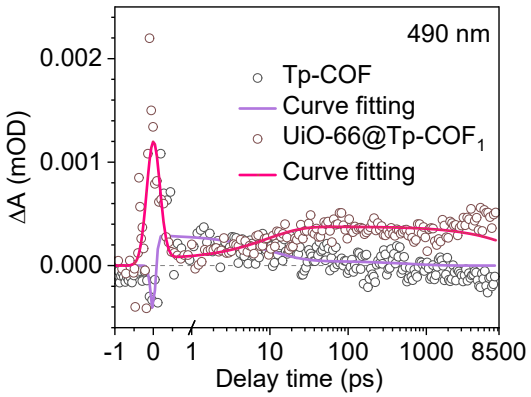

Fig. S16. The decay signals of Tp-COF and UiO-66@Tp-COF_1.

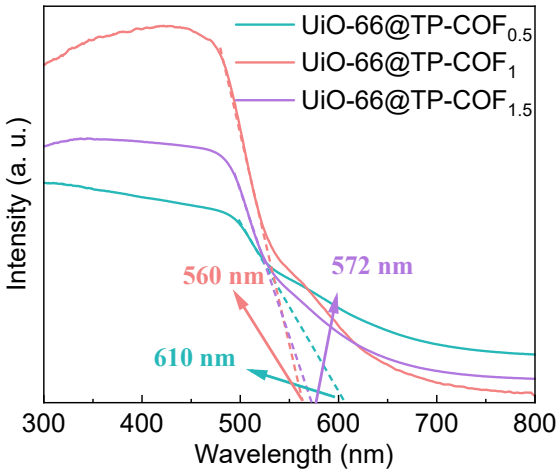

Fig. S17. UV-vis absorption spectra of UiO-66@Tp-COF_x.

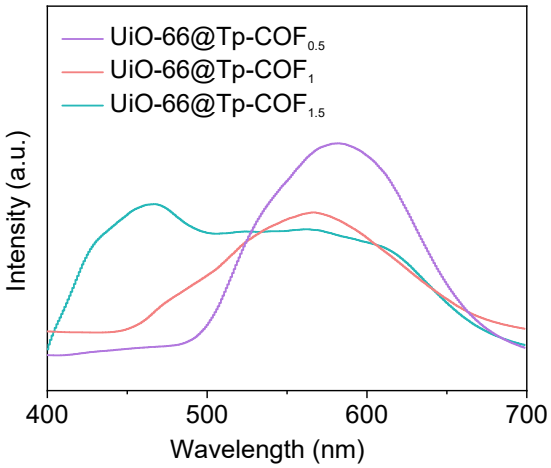

Fig. S18. Photoluminescence spectra (PL, excited at 375 nm) of UiO-66@Tp-COF_x.

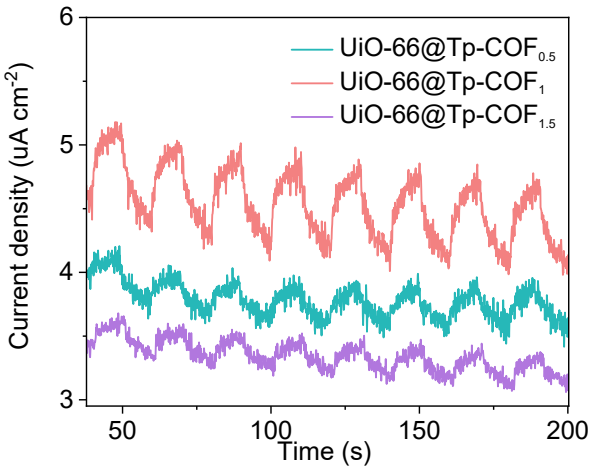

Fig. S19. Photocurrent response of UiO-66@Tp-COF_x.

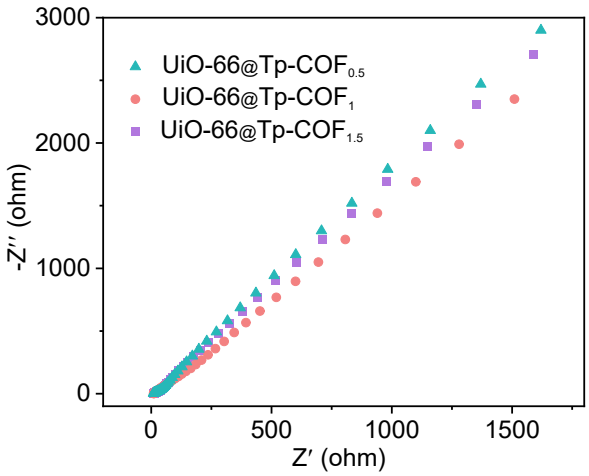

Fig. S20. EIS Nyquist plots of UiO-66@Tp-COF_x.

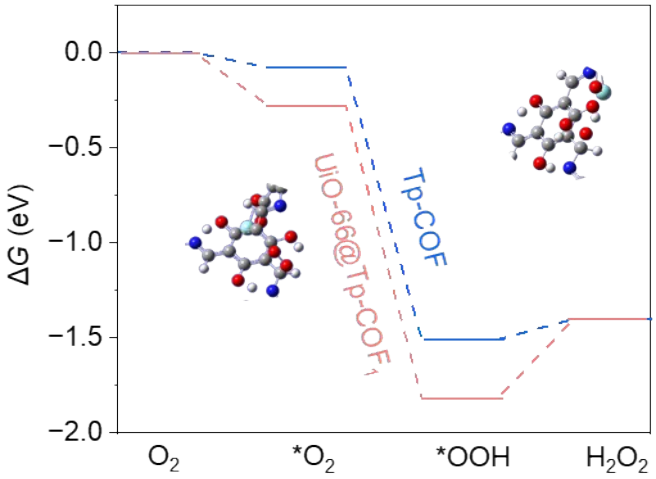

Fig. S21. Gibbs free energy diagrams of the O_2 photoreduction to H_2O_2 on Tp-COF and UiO-66@Tp-COF_1.

Table S1. Textural parameters of parent UiO-66, Tp-COF and UiO-66@Tp-COF_1.

Sample	S_{BET}* (m^2/g)	S_{mic}* (m^2/g)	S_{meso}/S_{BET} (%)	V_t* (cm^3/g)	V_{mic}* (cm^3/g)	V_{mic}/V_t(%)
UiO-66	947	913	96	0.37	0.34	92
Tp-COF	1046	807	77	0.64	0.35	55
UiO-66@Tp-COF_1	453	449	99	0.32	0.19	59

* S_{BET} and S_{mic} is the surface area of BET and mesoporous structure, respectively.

* V_t is the total volume. V_{mic} is mesoporous volume.

Table S2 Binding energy of peaks separated from N 1s spectra of Tp-COF and UiO-66@Tp-COF_x

Sample	Binding Energy			
	-NH-		-C=N-	
	Position (eV)	Content (%)	Position (eV)	Content (%)
Tp-COF	399.9	79.1	398.5	20.9
UiO-66@Tp-$COF_{0.5}$	399.7	62.8	398.3	37.2
UiO-66@Tp-COF_1	399.7	73.2	398.3	26.8
UiO-66@Tp-$COF_{1.5}$	399.7	89.8	398.3	10.2

References

[1] H. Yang, C. Li, T. Liu, T. Fellowes, S.Y. Chong, L. Catalano, M. Bahri, W. Zhang, Y. Xu, L. Liu, W. Zhao, A.M. Gardner, R. Clowes, N.D. Browning, X. Li, A.J. Cowan, A.I. Cooper, Packing-induced selectivity switching in molecular nanoparticle photocatalysts for hydrogen and hydrogen peroxide production, Nature Nanotechnology 18(3) (2023) 307-315. https://doi.org/10.1038/s41565-022-01289-9.

[2] M.J.T. Frisch, G.W. Schlegel, H.B. Scuseria, G.E. Robb, M.A. Cheeseman, J.R. Scalmani, G. Barone, V. Petersson, G.A. Nakatsuji, H. Li, X. Caricato, M. Marenich, A.V. Bloino, J. Janesko, B.G. Gomperts, R. Mennucci, B. Hratchian, H.P. Ortiz, J.V. Izmaylov, A.F. Sonnenberg, J. L. Williams-Young, D. Ding, F. Lipparini, F. Egidi, F. Goings, J. Peng, B. Petrone, A. Henderson, T. Ranasinghe, D. Zakrzewski, V.G. Gao, J. Rega, N. Zheng, G. Liang, W. Hada, M. Ehara, M. Toyota, K. Fukuda, R. Hasegawa, J. Ishida, M. Nakajima, T. Honda, Y. Kitao, O. Nakai, H. Vreven, T. Throssell, K. Montgomery, J.A. Jr. Peralta, J. E. Ogliaro, F. Bearpark, M.J. Heyd, J.J. Brothers, E.N. Kudin, K.N. Staroverov, V.N. Keith, T.A. Kobayashi, R. Normand, J. Raghavachari, K. Rendell, A.P. Burant, J.C. Iyengar, S.S. Tomasi, J. Cossi, M. Millam, J.M. Klene, M. Adamo, C. Cammi, R. Ochterski, J.W. Martin, R.L. Morokuma, K. Farkas, O. Foresman, J.B. Fox, D.J., Gaussian 16, Gaussian Inc.: Wallingford, CT (2016).

[3] A.D. Becke, Density-Functional Exchange-Energy Approximation with Correct Asymptotic-Behavior, Phys. Rev. A 38(6) (1988) 3098-3100. https://doi.org/10.1103/PhysRevA.38.3098.

[4] C.T. Lee, W.T. Yang, R.G. Parr, Development of the Colle-Salvetti Correlation-Energy Formula into a Functional of the Electron-Density, Phys. Rev. B 37(2) (1988) 785-789. https://doi.org/10.1103/PhysRevB.37.785.

[5] C. Chen, C. Wang, Y. Zhang, H. Sun, J. Xu, Y. Zhang, Y. Lou, Y. Zhu, C. Pan, Enhancing photocatalytic H_2O_2 production through the improvement of water oxidation via a novel lattice-oxygen-involved pathway, Applied Catalysis B: Environment and Energy 348 (2024) 123854. https://doi.org/https://doi.org/10.1016/j.apcatb.2024.123854.

[6] H. Zhang, W. Wei, K. Chi, Y. Zheng, X.Y. Kong, L. Ye, Y. Zhao, K.A.I. Zhang, Enhanced Photocatalytic Production of Hydrogen Peroxide by Covalent Triazine Frameworks with Stepwise Electron Transfer, ACS Catalysis 14(23) (2024) 17654-17663. https://doi.org/10.1021/acscatal.4c05328.

[7] L. Xu, K.S. Yeung, L. Li, X. Nan, O. Savateev, Z. Hu, J.C. Yu, Production of H2O2 via Energy Transfer Photocatalysis by Coupling with Furfuryl Alcohol Conversion over an Amide-Functionalized Heptazine Framework, Angewandte Chemie International Edition 24 (2025) e202504635. https://doi.org/https://doi.org/10.1002/anie.202504635.

[8] D. Wang, F. Tan, W. Zhao, S. Zhou, Q. Xu, L. Kan, L. Zhu, P. Gu, J. Lu, Develop Complex Photocatalytic System of D-π-A-type Conjugated Porous Polymers and Benzyl Alcohol Mediated Autocatalysis for Practical Artificial Photosynthesis of H_2O_2, Angewandte Chemie International Edition 64(23) (2025) e202425017. https://doi.org/https://doi.org/10.1002/anie.202425017.

[9] Y.-Y. Tang, X. Luo, R.-Q. Xia, J. Luo, S.-K. Peng, Z.-N. Liu, Q. Gao, M. Xie, R.-J. Wei, G.-H. Ning, D. Li, Molecular Engineering of Metal–Organic Frameworks for Boosting Photocatalytic Hydrogen Peroxide Production, Angewandte Chemie International Edition 63(36) (2024) e202408186. https://doi.org/https://doi.org/10.1002/anie.202408186.

[10] Q. Xue, H. Li, P. Jin, X. Zhou, F. Wang, Singlet-Oxygen-Driven Cooperative Photocatalytic Coupling of Biomass Valorization and Hydrogen Peroxide Production Using Covalent Organic Frameworks, Angewandte Chemie International Edition 64(19) (2025) e202423368. https://doi.org/https://doi.org/10.1002/anie.202423368.
[11] H. Zhang, Y. Zhu, Y. Sun, J. Khan, H. Liu, J. Xiao, H. Zhou, L. Han, Synergistic sulfur doping and nitrogen vacancies in porous graphite carbon nitride for enhanced photocatalytic H_2O_2 production, Journal of Environmental Chemical Engineering 11(5) (2023) 111122. https://doi.org/https://doi.org/10.1016/j.jece.2023.111122.
[12] Q. Wu, J. Cao, X. Wang, Y. Liu, Y. Zhao, H. Wang, Y. Liu, H. Huang, F. Liao, M. Shao, Z. Kang, A metal-free photocatalyst for highly efficient hydrogen peroxide photoproduction in real seawater, Nature Communications 12(1) (2021) 483. https://doi.org/10.1038/s41467-020-20823-8.
[13] Z. Jiang, J. Zhang, B. Cheng, Y. Zhang, J. Yu, L. Zhang, Hollow TiO_2@TpPa S-Scheme Photocatalyst for Efficient H_2O_2 Production Through $^1O_2$ in Deionized Water Using Phototautomerization, Small 21(8) (2025) 2409079. https://doi.org/https://doi.org/10.1002/smll.202409079.
[14] X. Wang, H. Li, S. Zhou, J. Ning, H. Wei, X. Li, S. Wang, L. Hao, D. Cao, Donor–Acceptor Fully Sp^2-Carbon Conjugated Covalent Organic Frameworks for Photocatalytic H_2O_2 Production, Advanced Functional Materials 24 2424035. https://doi.org/https://doi.org/10.1002/adfm.202424035.